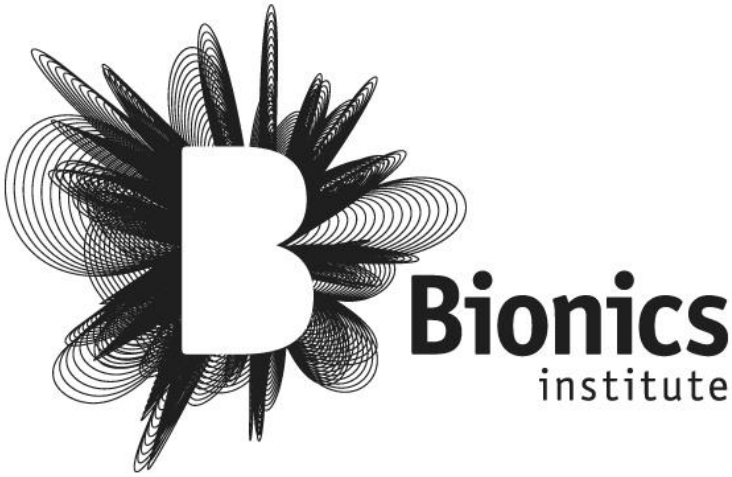

Articles in PresS. J Neurophysiol (October 10, 2007). doi:10.1152/jn.00629.2007

Inferior Colliculus Responses to Multichannel Microstimulation of the Ventral Cochlear Nucleus: Implications for Auditory Brainstem Implants

Mohit N. Shivdasani[1,2,3], Stefan J. Mauger[1,2,3], Graeme D. Rathbone[1,3] & Antonio G. Paolini[1,2]

[1]The Bionic Ear Institute, East Melbourne, VIC – 3002, AUSTRALIA

[2]School of Psychological Science, La Trobe University, VIC – 3086, AUSTRALIA

[3]Department of Electronic Engineering, La Trobe University, VIC – 3086, AUSTRALIA

Running Head: Midbrain Responses to Cochlear Nucleus Stimulation

Corresponding Author: Antonio G. Paolini,

Auditory Clinical Neuroscience Unit, The Bionic Ear Institute, 6th Floor Daly Wing,

St. Vincent's Hospital, Victoria Parade, Fitzroy, VIC – 3065, AUSTRALIA.

Email: tpaolini@bionicear.org

Tel: +61-3-92883515

Fax: +61-3-96677518

Abstract

Multichannel techniques were used to assess the frequency specificity of activation in the central nucleus of the inferior colliculus (CIC) produced by electrical stimulation of localized regions within the ventral cochlear nucleus (VCN). Data were recorded in response to pure tones from 141 and 193 multiunit clusters in the rat VCN and the CIC, respectively. Of 141 VCN sites, 126 were individually stimulated while recording responses in the CIC. A variety of CIC response types were seen with an increase in both electrical and acoustic stimulation levels. The majority of sites exhibited monotonic rate level types acoustically while spike rate saturation was achieved predominantly with electrical stimulation. In 20.6% of the 364 characteristic frequency aligned VCN-CIC pairs, the CIC sites did not respond to stimulation. In 26% of the 193 CIC sites, a high correlation was observed between acoustic tuning and electrical tuning obtained through VCN stimulation. A high degree of frequency specificity was found in 58% of the 118 lowest threshold VCN-CIC pairs. This was dependent on electrode placement within the VCN as a higher degree of frequency specificity was achieved with stimulation of medial, central and postero-lateral VCN regions than more antero-lateral regions. Broadness of acoustic tuning in the CIC played a role in frequency-specific activation. Narrowly tuned CIC sites showed the lowest degree of frequency specificity upon stimulation of the antero-lateral VCN regions. This data provides significant implications for Auditory Brainstem Implant electrode placement, current localization, power requirements and facilitation of information transfer to higher brain centers.

INTRODUCTION

The ventral cochlear nucleus (VCN) is the first processing site of sound information in the brain, and receives direct excitatory synaptic inputs from the cochlea via the auditory nerve (AN) (Lorente de Nó, 1933a, 1933b). The neurons of the VCN are arranged in a tonotopic order, with low frequency AN fibers innervating the most ventral and lateral regions of the VCN, and high frequency fibers innervating more dorsal and medial regions (Rose et al., 1959). On the basis of cytoarchitecture, there are several neuron types found in the VCN, each one different in anatomy (Osen, 1969; Hackney et al., 1990) and function (Evans and Nelson, 1973; Shofner and Young, 1985). The posteroventral cochlear nucleus (PVCN) in several animal species predominantly contains two types of cells that are known to project to higher auditory brain centers, such as the central nucleus of the inferior colliculus (CIC) of the midbrain, through both direct and polysynaptic pathways. (Osen, 1972; Beyerl, 1978; Adams, 1979a; Oliver, 1987; Cant, 1992; Schofield and Cant, 1996). One such type, the T-stellate neurons (also known as Type I multipolar neurons), are thought to be the prime encoders of monaural frequency (Osen, 1969; Brawer, 1974; Cant, 1981; Paolini et al., 2004; Paolini et al., 2005) and project directly to the CIC (Osen, 1972; Beyerl, 1978; Adams, 1979a; Oliver, 1987; Cant, 1992; Schofield and Cant, 1996). Another cell type, the octopus cells, are located in the most posterior regions of the PVCN and are a major source of inhibition to the CIC through the ventral nucleus of the lateral lemniscus (Friauf and Ostwald, 1988; Saint Marie and Baker, 1990; Adams, 1997; Schofield and Cant, 1997; Thompson, 1998; Nayagam et al., 2005, Nayagam et. al. 2006). The anteroventral cochlear nucleus (AVCN) is known to contain a high proportion of bushy cells (Harrison and Warr, 1962; Osen, 1969; Tolbert and Morest, 1982a, b), which do not directly project to the CIC (Adams, 1979b; Ryugo et al., 1981; Adams, 1983). However, these cells project to the superior olivary complex (Warr,

1966; Cant and Casseday, 1986), which in turn sends projections to the CIC (Browner and Webster, 1975; Roth et al., 1978).

In several animal species, the CIC is tonotopically arranged from low to high frequencies in a dorsomedial-ventrolateral direction (Aitkin et al., 1972; FitzPatrick, 1975; Semple and Aitkin, 1979; Huang and Fex, 1986). Although there are some differences in the anatomical characteristics of the VCN across species (Cant and Benson, 2003), given that both the VCN and the CIC are tonotopically organized, it is likely that the projections between the structures are frequency-specific, which is supported by previous anatomical studies (Osen, 1972; Oliver, 1987). What remains to be investigated is if these tonotopic projections are functionally valid for VCN stimulation. The knowledge gained by assessing this could provide significant further information on how to electrically stimulate the VCN with the Auditory Brainstem Implant (ABI).

The ABI differs from the Cochlear Implant (CI) in that it stimulates the surface of the cochlear nucleus (CN) rather than along the tonotopic gradient of the cochlea (Otto et al., 1998). Commercially available implants consist of either 12 (MED-EL C40+, MED-EL Corporation, Innsbruck, Austria) or 21 (Nucleus 24 ABI, Cochlear Ltd., Sydney, NSW, Australia) active stimulating electrodes fixed on a Dacron fabric mesh that fits on the surface of the CN in the lateral recess of the 4th ventricle. The ABI has mainly been used to restore hearing in patients with Neurofibromatosis Type II (NF2); a genetic condition usually marked by bilateral tumor growths on the VIIIth cranial nerve (Otto et al., 2002). Damage to this nerve following removal of these tumors may result in profound sensorineural hearing loss. Though patients with this condition are unable to benefit from the CI designed to stimulate the spiral ganglion neurons of the cochlea, they may benefit from stimulation of the VCN when

implanted with the ABI (Edgerton et al., 1982). In other conditions where a CI will not be effective, such as a temporal bone fracture with cochlear nerve avulsion, cochlear ossification, and possibly cochlear nerve aplasia, patients may also benefit from an ABI (Colletti and Shannon, 2005). When compared with CI recipients several clinical studies have shown that NF2 ABI users only obtain limited sound perception (Otto et al., 1998; Otto et al., 2002; Schwartz et al., 2003). The typical ABI user will benefit from environmental sound perception, however in most cases is unable to understand speech without lip-reading (Otto et al., 1998; Otto et al., 2002; Schwartz et al., 2003). A recent study (Colletti and Shannon, 2005) has reported that some non-NF2 patients can achieve significantly higher speech perception than NF2 patients. Although they suggested a separate pathway for speech and modulation coding, which might be damaged in NF2 patients, it is unclear why only some non-NF2 patients receive benefit.

Previous studies involving CIs (Friesen et al., 2001) and ABIs (Kuchta et al., 2004) have shown that the ability to perceive speech is largely correlated with the number of independent channels of frequency information. One way this may be achieved is by stimulation of localized groups of neurons within isofrequency laminae of the VCN. However, the present surface implant technology may have limited access to the tonotopic map located within the VCN. A penetrating electrode array may overcome this limitation as suggested by previous studies showing low thresholds, high dynamic ranges and topographic specificity in higher brain centers to VCN stimulation (El-Kashlan et al., 1991; McCreery et al., 1998; El-Kashlan, 1999; Takahashi et al., 2005, McCreery et. al. 2007).

In this investigation we examined the frequency specificity of activation of CIC neurons by microstimulation of the VCN across multiple sites. Our approach was to directly compare

CIC multiunit cluster responses obtained by electrical stimulation to those obtained acoustically. Unlike previous studies (El-Kashlan et al., 1991; McCreery et al., 1998; El-Kashlan, 1999; Takahashi et al., 2005, McCreery et. al. 2007), we stimulated specific frequency regions in the VCN, which were predetermined using acoustic stimulation. Multichannel electrodes were inserted in both structures along their tonotopic axes and after predetermining the characteristic frequencies (CFs) of the multiunit clusters at each electrode site, we stimulated each VCN site with single biphasic charge-balanced pulses. We recorded multiunit spike activity in the CIC and analyzed multiunit spike rate in response to stimulation, which allowed accurate measures of electrical thresholds, dynamic ranges and frequency specificity of activation. The hypothesis of our study was that CIC clusters respond with lowest current threshold to electrical stimulation of a frequency matched site in the VCN. We also hypothesized that this frequency specificity should depend on location of stimulation within the VCN. Our results have significant implications for ABIs.

MATERIALS AND METHODS

Surgery

Male Hooded Wistar rats (n = 8) weighing between 350-450 g were anaesthetized with Urethane in water (20% w/v, Sigma Aldrich, NSW, Australia) via the intra-peritoneal cavity. The animals were placed in a stereotaxic frame (David Kopf Instruments, Tujunga, CA) and fitted with hollow ear bars. Animal temperature was regulated at 37 degrees centigrade and monitored continuously using a DC homoeothermic blanket. Contralateral craniotomies were performed to access both the VCN and the inferior colliculus (IC). The cerebellum was aspirated after removing the outer duramater to expose the brainstem and VCN. Under visual control, using the lateral recess of the 4^{th} ventricle as a guide, 32-channel electrodes (Neuronexus Technologies, Ann Arbor, MI, USA) were inserted both into the ipsilateral (left) VCN and the contralateral (right) CIC along their tonotopic axes. In all experimental animals, the VCN electrodes were inserted in a caudo-rostral direction in order to access the central parts of the PVCN, which have a high concentration of T-stellate cells (See Results). The CIC electrodes for all experiments were inserted at a 10 degree rostro-caudal angle. A low impedance silver reference electrode was placed under the skin and served as a common reference for spike recording. All surgical procedures and protocols were approved by the La Trobe University Animal Ethics Committee (Protocol # 03/13) and the St. Vincent's Hospital Animal Ethics Committee (Protocol # 35/06).

Multichannel Electrodes

Each multichannel electrode consisted of four silicon substrate shanks (200 µm apart), each 5 mm long, attached to a fiberglass circuit board with eight iridium electrode sites (413 μm^2 surface area, 200 µm apart) on each shank (Referred to later as shanks a-d with sites 1-8 on

each shank; See Figures 1 & 2). Prior to each experiment, to increase their charge storage capacity, all 32 sites of the VCN electrode were electrochemically activated using cyclic voltammetry as described by Anderson et al. (1989) (CH Instruments, Inc., 660B Potentiostat and CHI200 Picoamp Booster, TX, USA). Upon activation, the impedance of each site was changed from 1 MΩ to less than 100 kΩ at 1 kHz, while each CIC electrode site had an impedance (unactivated) of 1-3 MΩ at 1 kHz.

Acoustic Protocols

All stimuli generation and data acquisition was performed using Tucker Davis Technologies System III hardware (TDT, FL, USA), with a custom-designed software package using TDT's OpenEx client-server applications. Acoustically driven units were first located in both structures by presenting a broadband (1 – 44 kHz) Gaussian distributed noise stimulus (50 ms bursts, 500 ms inter-trial interval) while advancing the electrode arrays into the VCN and CIC using a motorized micro-drive (Sutter Instruments, USA). Once the arrays were in position, responses to various pure tones (1 – 44 kHz, 1 kHz steps, 50 ms bursts, 300 ms inter-trial interval) of different amplitudes (10 – 70 dB sound pressure level (SPL), 10 dB steps) were obtained in order to generate a response area for each recording site (10 repetitions for each frequency-intensity combination). Ear bars were calibrated prior to each experiment using a 1/8-inch Brüel & Kjær microphone and measuring amplifier unit (Nærum, Denmark).

Electrical Protocols

Each acoustically driven electrode site in the VCN was electrically stimulated with charge-balanced biphasic current pulses using the site above it on the same shank as a reference (120 μs per phase, 80 μs interphase gap, bipolar configuration). For the topmost site on each shank, the site immediately below it was used as a reference. Microstimulators (32-channel

RX7 micro stimulators, TDT, FL, USA) were used to deliver currents up to 100 µA (typically maximum current delivered was 54 µA). The pulse rate on every channel was fixed to one pulse every 500 ms (50 repetitions for each current amplitude). Since the electrode sites had a surface area of 413 μm^2 and our stimulus pulses were 120 µs per phase, even at 100 µA, the maximum charge density was 2.9 mC/cm^2 and the charge per phase was 12 nC. This ensured that we were not above the electrochemical charge injection limit for iridium oxide (approximately 3 mC/cm^2) (Beebe and Rose, 1988) and that we did not cause any neural damage. McCreery et. al. (1990) showed that charge per phases of up to 5000 nC could be used safely with the charge density set at 10 $\mu C/cm^2$ and the pulse width set to 400 µs per phase at a stimulation rate of 50 Hz. At our stimulation rate (2 Hz), the threshold of damage would be even higher. Moreover, at the end of the stimulation paradigm in each experiment, acoustic response areas were repeated to ensure that the VCN neurons were still functional and showed similar tuning properties.

Data Acquisition

Data was acquired at a sampling rate of 24.4 kHz using an online threshold based spike discriminator. In order to determine when spikes occurred, the incoming signal on each channel was monitored in a two-second window to get an estimate of the spontaneous baseline level of activity. If the signal crossed this baseline activity by more than 4.2 standard deviations, a spike detector was triggered, which recorded the next 31 samples (1.2 ms) of the signal waveform (bandpass filtered from 300 - 5000 Hz) along with a timestamp value indicating the time of occurrence of the largest positive or negative peak of the spike. After recording 31 samples, the spike detector could be triggered again.

Data Analysis

Initial Procedure. Multiunit activity from each of the electrode sites was analyzed offline, using programs we developed in Matlab (The Mathworks, USA). A typical approach to analyze multiunit recordings is spike sorting (Lewicki, 1998). One of the major challenges for any sorting technique has been to distinguish spike waveforms that occur as a result of two or more neurons firing simultaneously, resulting in fully or partially overlapping spikes (Bar-Gad et al., 2001). In structures like the VCN and the CIC, it is expected that when an acoustic stimulus is presented, not only one but several neurons close to a recording site will respond simultaneously. Therefore, it was not possible to determine whether any spike waveform acquired by our system corresponded to a single neuron's spike, hence we analyzed all our data using the multiunit activity from each site. Also, the method of online spike detection meant that while the spike detector was recording a waveform, it could not be triggered by another spike until it had recorded 31 samples of the signal. This could result in the recording system not accurately keeping track of all the spikes, especially those which occurred very near in time to each other. Therefore, a re-thresholding procedure was used offline to accurately determine the occurrence of spikes. This procedure involved finding the mean and standard deviation of each 31-sample spike recorded by the system, and then checking how many times any particular sample out of the 31 exceeded 1.5 standard deviations above the mean. Each threshold crossing was picked up by a Schmitt trigger function, which kept track of the occurrence of spikes. This provided a more accurate estimate for spike rate calculations for analysis of the data.

Acoustic Response Areas. Spike rate calculations were made for each frequency-amplitude combination of sound presented using a time window 0-50 ms from the stimulus onset. These

were then plotted as a function of frequency and intensity to give a response area for each of the 64 recorded sites in the two structures. The CF for each site in the VCN and the CIC was determined from its response area as the frequency which elicited maximum activity at the lowest threshold (dB SPL). Acoustic threshold was determined by visual inspection of the Peri Stimulus Time Histograms (PSTHs) and by selecting the dB SPL where spike discharge significantly increased above spontaneous levels within a window of 0 – 50 ms from stimulus onset.

Electrical Response Areas. In order to directly compare CIC responses to electrical and acoustic stimulation, spike rate calculations in response to electrical stimulation were made using a window of 2 – 25 ms from stimulus onset. This ensured that the stimulus artifact recorded in the CIC would not be counted in the calculations. By plotting these spike rates as a function of the current amplitude and CF of each stimulated VCN site, we were able to generate an electrical response area (See Results) for each CIC site and compare its tuning characteristics directly to the tuning characteristics of the acoustic response area.

Electrical Threshold, Saturation & Dynamic Range. Methods to obtain electrical thresholds vary and range from visual inspection of the PSTHs to curve fitting incorporating spontaneous and maximum firing rates. For our data, we chose an objective mathematical method described by Koppl and Yates (1999) and Nizami (2002). This method calculates the thresholds along with saturation firing rates and therefore dynamic ranges can also be found. First, a least-squares regression method was used to fit a sigmoid to the stimulus level versus firing rate plots for all electrically evoked responses. Endpoints of the dynamic range were then determined by calculating the current levels required to produce firing rates 10% above threshold and 10% below saturation (Koppl and Yates, 1999; Yates et al., 2000; Nizami,

2002). This method was selected as it has been shown to successfully model mammalian and avian AN rate-level functions (Sachs and Abbas, 1974; Sachs et al., 1989; Yates, 1990; Koppl and Yates, 1999; Yates et al., 2000) and the threshold and saturation estimates obtained from our data using this method, matched well to the values obtained by visual inspection of the electrical PSTHs. Dynamic ranges are presented in μA and in dB.

Histological Analysis

At the end of each experiment, the animal was deeply anesthetized and perfused transcardially using 0.1 M phosphate buffered saline and 10% neutral buffered formalin (Sigma Aldrich, NSW, Australia). Following tissue fixation, the brain was removed and snap-frozen. Serial coronal sections of 60 μm were collected using a freezing sledge microtome (Thomas Scientific, Swedesboro, NJ, USA). Sections were placed on gelatin-coated slides, stained with Thionine and cover-slipped. Positions of the electrodes through the VCN and CIC were confirmed using bright field microscopy and VCN shank locations were reconstructed by manual drawings using a combination of histological data and known visual placements of the electrodes. Outlines of the CN were determined in the horizontal and parasagittal planes with reference to the rat brain atlas (Paxinos and Watson, 2005). Upon viewing the coronal histological sections, the placement of the VCN probe was estimated and dots representing the shanks were added to the outlines giving a relative indication of where the VCN electrodes were placed within the boundaries of the model outlines (See Figure 1). Histological data was obtained in six out of the eight experimental animals. Due to multiple VCN penetrations, histological data could not be verified for the remaining two animals.

RESULTS

Tonotopic Maps & Histological Results

Figure 1A summarizes the placement of electrode shanks at their entry point into the CN in the horizontal plane. In four of the six animals, electrodes were inserted either towards the medial edge or the lateral edge of the VCN while in two animals, placements were made in the central regions of the VCN. In one experiment (07_007), although the electrode was inserted into the dorsal CN (DCN) at its entry point, it was inserted with a greater caudo-rostral angle as compared to the other experiments. As a result, few of the dorsally located electrode sites from this experiment were either in the DCN or close to the granule cell lamina between the DCN and the VCN (indicated in Figure 1B, black dotted lines). However, the electrode sites used for stimulation in this experiment were located in the VCN. Multiunit activity was recorded from individual sites located within the VCN across the tonotopic plane; low frequency sensitive neurons in the ventral regions and high frequency sensitive neurons in more dorsal regions (Figure 1B (i-vi)). Minimal tissue damage was noted in the VCN as a result of these penetrating electrode shanks by visual inspection of the histological sections close to where the electrode tracks were seen (Figure 1C i-ii). Electrode placements in the IC were verified histologically within its central nucleus (Figure 2, Paxinos & Watson, 2005). Multiunit activity recorded across the CIC showed the extent of the tonotopic gradient with clusters sensitive from low frequencies to high frequencies in the dorso-ventral direction.

Characteristics of VCN Electrical Stimulation

In 334 of 512 possible sites (32 sites in each structure, 8 animals), multiunit cluster responses to frequencies at multiple intensity levels were obtained (response areas; 141, VCN; 193,

CIC). Since our experiments involved sophisticated methods of surgery and recording techniques, due to experimental constraints it was on occasion not possible to stimulate all VCN sites in given experiment. Of the VCN sites, 126 (89.4%) were electrically stimulated, of which 100 initiated a response in the CIC. The remaining 26 VCN sites did not show any response in the CIC even when stimulated at the highest current amplitude (100 μA). For the CIC, all 193 sites showed a response to electrical stimulation of at least one site in the VCN. In order to further analyze CIC responses to VCN stimulation, electrode sites in both structures were paired according to their CF. Those CIC sites which had a CF equal to or 1 kHz away from VCN sites in a given experiment were classified together in one group called "CF Aligned". The other group consisted of CIC sites that responded with the lowest threshold to stimulation of a single VCN site. These were classified into the "Lowest Threshold Aligned" group, consistent with Lim and Anderson (2006). VCN sites that did not have a CF matched site in the CIC (n = 32) were not paired with any CIC sites and not included in the analysis. For both the groups, analyses were performed on the data obtained from stimulation of 68 VCN sites.

A total of 364 VCN-CIC pairs belonging to the CF Aligned group were analyzed for electrical stimulation (Figure 3). In response to increasing levels of both acoustic and electrical stimulation, CIC sites exhibited an increase in discharge (Figure 3A, 3B) with multiunit spike activity generally observed between 4 and 60 ms from stimulus onset. In contrast to acoustic stimulation, a well-timed onset peak was seen with higher stimulus currents in PSTHs from electrical stimulation, 4-5 ms from stimulus onset (Figure 3B), possibly a result of antidromic activation in the VCN.

In a given experiment, it was possible for multiple VCN sites to have a similar CF, thus a given CIC site may have been paired to more than one site in the VCN. The CIC sites belonging to these pairs did not necessarily respond with the same threshold to stimulation of their VCN counterparts (Figure 3F). Of the 364 CF matched pairs analyzed, 289 (79.4%) responded to VCN stimulation. A total of 142 CIC sites were part of these responding pairs. The remaining 75 VCN-CIC pairs (20.6%) gave no response, the majority of which (45.3%) had electrode sites located in more antero-lateral regions of the VCN (Exp 06_028 & Exp 07_005), as shown in Figure 4. A total of 51 CIC sites made up these non-responding pairs. However, 29 (57%) of these 51 CIC sites responded to stimulation of another CF matched VCN site and thus were part of the 289 responding pairs. From the CIC sites that responded to stimulation, we were able to plot spike discharge as a function of stimulus current and designated CFs of stimulated sites within the VCN to construct electrical response areas (Figure 3H, Figure 5), the tuning characteristics of which could be compared directly to those of the acoustic response (See “Electrical Thresholds versus Acoustic Thresholds” section below).

Differing rate-level functions were recorded from CIC multiunit clusters to stimulation of CF aligned VCN sites (Figure, 3G). The shape of the rate-level function was used to classify multiunit cluster responses into four categories: monotonic, plateau, non-monotonic and complex (Aitkin, 1991; Figure 6). Monotonic responses (Figure 6A(i) and 6B(i)) were classified in cases where spike rates did not reach a saturation level and kept increasing with stimulus levels, whereas those that did saturate were classified as plateau type responses (Figure 6A(ii) and 6B(ii)). Non-Monotonic responses (Figure 6A(iii) and 6B(iii)) were classified in cases where spike rates first increased with stimulus levels but dropped below 50% of the maximum spike rate at higher stimulus levels. A final group of multiunit clusters

exhibited both monotonic and non-monotonic rate-level characteristics (Figure 6A(iv) and 6B(iv)), which were classified as complex responses. The distribution of all response types seen with both acoustic (n = 138) and electrical (n = 289) stimulation is shown in Figure 6C. In most CIC multiunit clusters (56.5%), acoustic rate-level functions did not reach a saturation point (Figure 6C left). This was in contrast to that seen upon electrical stimulation of CF aligned sites where the majority of clusters (63.7%) exhibited spike rate saturation over our typical stimulated current range (0-54 μA; Figure 6C right).

The distribution of all orthodromically activated thresholds, saturation points and dynamic ranges obtained from the electrical rate-level functions of all VCN-CIC pairs is shown in Figure 7. The method to obtain electrical thresholds and saturation points described earlier was applied to all responses regardless of the type of rate-level function. For monotonic responses, the saturation point was chosen as the highest current level in our range. For non-monotonic and complex responses, the saturation point was chosen as the current level that elicited the overall maximum spike rate. The mean threshold ± standard deviation for the pairs belonging to the CF Aligned group (n = 289, Figure 7A (i-iv)) was found to be 17.24 ± 11.34 μA and mean dynamic range was 12.44 ± 9.64 μA (5.17 ± 2.95 dB). The Lowest Threshold Aligned group consisted of VCN-CIC pairs (n = 118) that were most sensitive to stimulation of a single VCN site. This group gave a lower mean threshold than the CF Aligned group (12.63 ± 10.11 μA) and a mean dynamic range of 11.39 ± 10.22 μA (6.23 ± 3.68 dB) (Figure 7B i-iv).

The threshold of the presumed antidromic activation (arrow in Figure 3B) was noted as the current level, which first elicited the time locked onset peak that continued to be present at all current levels above threshold. Although the timely locked nature and the sudden appearance

of activity above threshold are shown to be representatives of antidromic activity (Swadlow, 1974; Swadlow et al., 1978; Lim and Anderson, 2007) these properties are not always sufficient to discern antidromic spikes from orthodromic spikes, hence we labeled our responses as "presumed" antidromic activity. Of 1313 total CIC responses to stimulation of the 100 VCN sites, 565 responses (43%) showed the presence of antidromic activity. In 541 (96%) of these responses, the threshold of antidromic activity to VCN stimulation was found to be equal to or higher than the threshold of the delayed orthodromic activity. Mean electrical threshold of all antidromic responses was found to be 30.72 ± 13 μA (Mean ± Standard Deviation). While we have included these responses in our analysis, they did not impact upon our overall threshold measures.

Electrical Thresholds versus Acoustic Thresholds

In order to directly compare the acoustic and electrical tuning at threshold levels for all CIC sites, both on-CF and off-CF, we plotted regression lines for the thresholds elicited by acoustic stimulation at given frequencies against the electrical thresholds elicited by stimulation of VCN sites with CFs equal to those frequencies (Figure 8). Only CIC sites that responded to stimulation of at least three VCN sites were analyzed (n = 135), of which 25.93% exhibited a high correlation (Pearson's coefficient of correlation, $r > 0.7$) while 11% showed moderate correlation ($0.5 < r \leq 0.7$) between acoustic and electrical thresholds (Hinkle et al., 1998). Negatively correlated sites accounted for approximately 35% of the total number while 20% of the total sites fell in the -0.2 to -0.5 range (Figure 8I). As seen from the single experiment plots in Figure 8 A-H, the majority of negatively correlated CIC sites came from two experiments with centrally located VCN electrode positions (Figure 1, Exp 06_002 & Exp 06_003) while the remaining experiments had CIC sites that showed positive correlation between acoustic and electrical thresholds.

Frequency Specificity of CIC Activation

The data were analyzed on a VCN shank by shank basis across all experiments to test if location of VCN stimulation correlated with the degree of frequency-specific CIC activation. For each VCN site stimulated that had at least one CF matched site in the CIC (n = 68), the tonotopic gradient of the CIC was examined for the lowest threshold response (Figure 9A). For a perfect tonotopic point to point mapping between the VCN and the CIC, each frequency region in the VCN when stimulated should elicit the lowest threshold response in the same frequency region in the CIC (Figure 9A, Solid line). For each point in Figure 9A, the frequency difference between the stimulated VCN site and the lowest threshold CIC site was calculated. The average frequency difference for each VCN shank was used as a measure of shank effectiveness in eliciting frequency-specific CIC activation. VCN shanks with at least 67% of the lowest threshold VCN-CIC pairs that had frequency differences of less than or equal to 3 kHz were classified into the "Group 1 shanks" (closed circles, Figure 9A, 9B). Remaining VCN shanks were classified into a second group ("Group 2 shanks", open circles, Figure 9A, 9B). The overall degree of frequency-specific CIC activation was found to be higher for the Group 1 shanks, which were placed more centrally, on the medial edge or more posterior in the VCN while more lateral and anterior VCN placements (Group 2 shanks) showed a lower degree of frequency specificity (Figure 9C).

Frequency specificity was also maintained at higher current levels. Figure 9D shows the CF of each CIC site plotted against the CF of the VCN site that elicited maximum spike discharge on that CIC site across all current levels, 2-25 ms from stimulus onset. Only CIC

sites that had at least one CF matched VCN site were analyzed (n = 96). Most CIC sites (69.8%) responded with maximum spike discharge to stimulation of VCN sites belonging to the Group 1 shanks. Mean frequency difference for these maximum discharge VCN-CIC pairs was 4.6 ± 5.2 kHz. Fewer CIC sites responded with maximum discharge to stimulation of VCN sites, which were either on the Group 2 shanks (11.5%; Mean frequency difference = 5.5 ± 3.8 kHz), or on shanks with unknown placements (18.7%; indicated by crosses; Mean frequency difference = 6.7 ± 4.7 kHz).

In addition to being frequency-specific, the mean threshold elicited in the CIC for the Group 1 shanks (12.8 ± 6.4 μA) was found to be significantly lower ($p < 0.001$) than the mean threshold for the Group 2 shanks (21.2 ± 11.5 μA). The mean dynamic range was found to be larger ($p < 0.001$) for the Group 2 shanks (6.67 ± 3.2 dB) as compared to the Group 1 shanks (4.93 ± 2.7 dB) (Figure 9E, 9F; Mean ± Standard Deviation).

Effect of Broadness of Tuning on Frequency Specificity

Figure 10 shows the relationship between changes in electrical thresholds for all CIC sites from the threshold of a CF matched VCN-CIC pair, plotted against their corresponding frequency differences from the VCN site in that pair. In cases where there was more than one CF matched CIC site for a given VCN site, the change in threshold was calculated from the one that responded with lowest threshold.. From the acoustic response area of each CIC site, the Quality factor at 10 dB above threshold (Q_{10}) was calculated as the CF divided by the bandwidth in kHz, as a measure of sharpness of tuning (Kelly et al., 1991). Sites that gave a Q_{10} less than or equal to one (n = 72) were classified as broadly tuned while those with a Q_{10} above one (n = 121) were classified as narrowly tuned. For the CIC sites that responded to VCN sites in the Group 1 shanks, both broadly tuned (Figure 10 A1, A2) and narrowly tuned

(Figure 10 B1, B2) CIC sites showed a trend for threshold differences to increase with a rise in frequency difference (Narrowly tuned, $r = 0.41$, $p < 0.01$; Broadly tuned, $r = 0.27$, $p < 0.01$). For the Group 2 shanks, only the broadly tuned CIC sites exhibited this trend of increasing threshold differences with increasing frequency differences ($r = 0.22$, $p < 0.05$).

DISCUSSION

In this investigation, we examined the spatial distribution of excitation within the CIC, evoked by electrical stimulation of selective VCN sites. Given that VCN neurons project monosynaptically as well as polysynaptically to contralateral CIC neurons (Cant and Benson, 2003), and in a tonotopic manner based on anatomical studies (Osen, 1972; Oliver, 1987), we expected that CIC neurons would be most sensitive to stimulation of VCN neurons with the same CF and conversely, less sensitive to stimulation of neurons with different CFs. In support of this, a high degree of frequency specificity was seen in VCN-CIC pairs between the CFs of regions activated in the CIC with lowest threshold and CFs of regions stimulated in the VCN. This frequency specificity was not only present at threshold levels but was maintained across all current levels in our stimulation range. A major factor contributing to this high degree of frequency specificity was the placement of the electrodes within the VCN. Best results were obtained when electrodes were placed towards the medial, central or postero-lateral regions rather than more antero-lateral regions of this nucleus.

The postero-lateral and central placements would stimulate regions within the PVCN where a high concentration of T-stellate cells are found (Smith and Rhode, 1989). Moreover, a high proportion of CIC sites exhibited maximum spike discharge to stimulation of the central and postero-lateral VCN regions, which is consistent with a large number of T-stellate cell projections arising from these regions that correspond to the main excitatory inputs to the contralateral CIC. Medial and few of the extreme lateral placements close to the free surface of the VCN would most likely stimulate the granule cell domain (Mugnaini et al., 1980b; Mugnaini et al., 1980a; Weedman et al., 1996). These cells are known to project to the fusiform cells (also known as pyramidal cells) of the DCN (Mugnaini et al., 1980b; Ryugo et

al., 1995), which in turn project to the CIC (Berrebi and Mugnaini, 1991). The medial extent of the granule cell domain is more developed in rats (Mugnaini et al., 1980b), thus increasing the likelihood of granule cell stimulation with medial shank placements in our experiments.

In contrast, the antero-lateral placements would predominantly excite the AVCN, which is known to contain a high proportion of bushy cells (Harrison and Warr, 1962; Osen, 1969; Tolbert and Morest, 1982a, b). As bushy cells do not project directly to the CIC (Adams, 1979b; Ryugo et al., 1981; Adams, 1983), higher levels of current would be required to evoke a CIC response for these antero-lateral placements as current spreads to neighboring T-stellate regions. This indiscriminant activation of VCN T-stellate neurons may explain the high proportion of unmatched VCN-CIC pairs with lowest threshold from antero-lateral VCN placements. This was manifested predominantly in narrowly tuned CIC neurons while broadly tuned neurons were generally unaffected. This alludes to the possibility that narrowly tuned CIC neurons may receive projections from the narrowly tuned T-stellate neurons of the PVCN, while broadly tuned CIC neurons may receive polysynaptic projections from a wide variety of cells types, including those from the AVCN. Furthermore, a large proportion of these antero-lateral placements did not elicit a response in CF aligned VCN-CIC pairs and very few CIC sites responded with maximum spike discharge to stimulation of these regions. This suggests that the current spread from these placements was confined to the AVCN. It is possible that in those cases, even the highest current amplitude (54 μA) was not enough for current to spread to the central PVCN T-stellate regions.

From a CIC perspective, over a third of the CIC sites analyzed showed a moderate to high correlation between their acoustic tuning and electrical tuning. However, for CIC sites in the experiments that had central VCN placements, a poor correlation was observed (Exp 06_002

& 06_003). In these experiments, we found that although lowest threshold was obtained by stimulating a CF matched site in the VCN, when VCN sites away from CF were stimulated, the thresholds did not increase substantially. One possible explanation for this could be related to the nature of current spread in the VCN. Central regions of the VCN are known to have a high proportion of AN fibers entering via the AN trunk (Lorente de Nó, 1933a, 1933b; Osen, 1970; Arnesen and Osen, 1978; Arnesen et al., 1978). The high probability of stimulating these fibers of passage may affect electrical tuning in the CIC at higher current levels.

Electrical stimulation thresholds obtained in our study were consistent with the results obtained by McCreery et. al. (2000) who obtained CIC activation through chronic VCN stimulation at current levels as low as 6 μA. We also found that two VCN sites within an experiment that had the same CF as a CIC site, elicited different electrical threshold values and some VCN sites when stimulated, did not elicit any response in CF matched CIC sites. This lack of stimulus driven activity in higher order auditory structures resulting from stimulation of some CN sites was also noted by Takahashi et al. (2005) who observed a lack of auditory cortical activation from a large proportion of CN sites. In this paradigm, we made use of bipolar stimulation in order to minimize current spread across frequency laminae. It is possible that neurons within the CIC receive convergent input from several points within a VCN isofrequency lamina. It is unknown whether it is sufficient to only stimulate a part of an isofrequency lamina to convey meaningful frequency information in higher order centers. There may be benefit in stimulating a greater number of sites within an isofrequency lamina to maximize frequency-specific activation in the CIC.

Back-propagation of fibers may also influence the responses obtained within the CIC to electrical stimulation of the VCN. Multiunit clusters in the CIC often exhibited a well-timed onset response to VCN electrical stimulation, which occurred at latencies in the order of 4-5 ms from stimulus onset. This time-locked onset response may be a result of antidromic activation of descending projections known to exist from the IC to the CN (Faye-Lund, 1988; Schofield and Cant, 1999; Schofield, 2001; Coomes and Schofield, 2004; Okoyama et al., 2006).

Implications for an ABI

Our study examined the degree of frequency specificity of CIC activation achievable via electrical stimulation of the VCN. The results of this study are directly applicable to the development of ABIs. We have identified the following four major implications from our research.

VCN Electrode Placement. The need for the electrodes to access the tonotopic organization of the VCN is an important consideration in achieving better performance. Based on our results, it is evident that the placement of the implant array into the VCN is a critical factor in conveying frequency-specific information to higher order brain centers. We have shown using a penetrating electrode array that medial, central and postero-lateral regions of the VCN when stimulated produce greater frequency-specific CIC activation as compared to the antero-lateral regions. This is consistent with McCreery et al. (1998) who showed that central regions of the PVCN are suitable for penetrating ABI implantation and McCreery et. al. (2007) who recently showed that the rostral-lateral and rostral-medial region of the VCN when stimulated chronically elicited significantly lower degrees of CIC frequency specificity as compared to the caudal-lateral and caudal-medial VCN regions. Based on our results if a

surface array is placed on the postero-lateral surface of the VCN in a dorso-ventral direction using the present commercial ABI, some frequency-specific stimulation may be achievable but a penetrating array in the PVCN would result in an increased likelihood of frequency-specific CIC activation. However, a correct placement of the electrode array is not sufficient on its own to guarantee best results. One must consider the effects of deafness periods on the structure and function of the VCN. Hearing loss can evoke significant morphological and physiological changes within the auditory brainstem, and these changes become greater with duration of deafness (Hardie and Shepherd, 1999). In particular, hearing loss is associated with a reduction in overall CN volume and an increase in neural density (Hardie and Shepherd, 1999), which are likely to impact on the effectiveness of the ABI.

Current Localization. We have shown some similarity between electrical and acoustic response areas in the CIC but this was not found in all cases. In fact, regardless of whether CIC neurons were broadly or narrowly tuned acoustically, they responded with similar thresholds to stimulation of VCN regions within a two kHz range for our classified Group 1 shanks, which were placed medially, centrally or postero-laterally in the VCN. For the Group 2 shanks which were placed more antero-laterally, similar threshold CIC activation was within a 6 kHz range. Although bipolar stimulation of the VCN was implemented using electrode sites with relatively small surface areas, we did not always achieve localized, frequency-specific CIC activation. Perhaps more sophisticated methods like tripolar or even quadropolar stimulation (Jolly et al., 1996) or using different pulse widths and shapes may be an advantage over bipolar stimulation. However, one must consider to what extent stimulation of passing fibers might be a limiting factor in achieving frequency-specific activation.

We realize that our results were obtained by stimulating a rat VCN, where the frequency laminae would be less widespread as compared to a human and in addition, the electrode dimensions that we used in this study were in the order of micrometers instead of millimeters. Humans and several other primate species have their best hearing frequencies (indicated by audiograms) centered around 4-8 kHz and the upper hearing limit of most humans is centered around 17 kHz (Heffner, 2004). This is in contrast to the rat, which has an upper hearing limit of up to 80 kHz (Kelly and Masterton, 1977). Hence, we would expect the human VCN to have a tonotopic map with frequencies shifted towards lower frequency scales compared to the rat.

ABI Power Requirements. Our results using penetrating electrodes show that charge deliveries as low as 0.36 nC (3 μA, 120 μs per phase) are sufficient to elicit a frequency-specific response in the CIC. Present surface electrodes have been reported to elicit thresholds in the order of 2 nC (Colletti and Shannon, 2005). CIC multiunit clusters in our study exhibited average spike rate saturation at current levels close to 30 μA. These results imply that a penetrating ABI would have more efficient power requirements.

Facilitation of Information Transfer. A final implication of our results is that not all acoustically driven VCN stimulation sites when electrically stimulated produced a response in the CIC. This implies a need for an electrode design which will incorporate sufficient redundancy to optimize performance. In addition, individual stimulation of two or more VCN areas with similar CFs often elicited different thresholds and different rate level functions in the CIC. We propose that a greater number of electrode sites will not only provide sufficient redundancy but also allow stimulation of multiple sites within VCN isofrequency laminae to maximize frequency-specific CIC activation.

REFERENCES

Adams JC. Identification of cochlear nucleus projections by removal of HRP reaction product. *Brain Res* 177:165-169, 1979a.

Adams JC. Ascending projections to the inferior colliculus. *J Comp Neurol* 183:519-538, 1979b.

Adams JC. Multipolar cells in the ventral cochlear nucleus project to the dorsal cochlear nucleus and the inferior colliculus. *Neurosci Lett* 37:205-208, 1983.

Adams JC. Projections from octopus cells of the posteroventral cochlear nucleus to the ventral nucleus of the lateral lemniscus in cat and human. *Auditory Neurosci* 3:335-350, 1997.

Aitkin L. Rate-level functions of neurons in the inferior colliculus of cats measured with the use of free-field sound stimuli. *J Neurophysiol* 65:383-392, 1991.

Aitkin LM, Fryman S, Blake DW, Webster WR. Responses of neurones in the rabbit inferior colliculus. I. Frequency-specificity and topographic arrangement. *Brain Res* 47:77-90, 1972.

Anderson DJ, Najafi K, Tanghe SJ, Evans DA, Levy KL, Hetke JF, Xue XL, Zappia JJ, Wise KD. Batch-fabricated thin-film electrodes for stimulation of the central auditory system. *IEEE Trans Biomed Eng* 36:693-704, 1989.

Arnesen AR, Osen KK. The cochlear nerve in the cat: topography, cochleotopy, and fiber spectrum. *J Comp Neurol* 178:661-678, 1978.

Arnesen AR, Osen KK, Mugnaini E. Temporal and spatial sequence of anterograde degeneration in the cochlear nerve fibers of the cat. A light microscopic study. *J Comp Neurol* 178:679-696, 1978.

Bar-Gad I, Ritov Y, Vaadia E, Bergman H. Failure in identification of overlapping spikes from multiple neuron activity causes artificial correlations. *J Neurosci Methods* 107:1-13, 2001.

Beebe X, Rose TL. Charge injection limits of activated iridium oxide electrodes with 0.2 ms pulses in bicarbonate buffered saline. *IEEE Trans Biomed Eng* 35:494-495, 1988.

Berrebi AS, Mugnaini E. Distribution and targets of the cartwheel cell axon in the dorsal cochlear nucleus of the guinea pig. *Anat Embryol (Berl)* 183:427-454, 1991.

Beyerl BD. Afferent projections to the central nucleus of the inferior colliculus in the rat. *Brain Res* 145:209-223, 1978.

Brawer JR, Morest DK, Kane, EC. The neuronal architecture of the cochlear nucleus of the cat. *J Neurophysiol* 155:251-300, 1974.

Browner RH, Webster DB. Projections of the trapezoid body and the superior olivary complex of the Kangaroo rat (Dipodomys merriami). *Brain Behav Evol* 11:322-354, 1975.

Cant NB. The fine structure of two types of stellate cells in the anterior division of the anteroventral cochlear nucleus of the cat. *Neuroscience* 6:2643-2655, 1981.

Cant NB, Casseday JH. Projections from the anteroventral cochlear nucleus to the lateral and medial superior olivary nuclei. *J Comp Neurol* 247:457-476, 1986.

Cant NB. The cochlear nucleus: neuronal types and their synaptic organization. In: *The Mammalian Auditory Pathway: neuroanatomy*, edited by Webster DB, Popper AN, Fay RR. New York: Springer-Verlag, 1992, pp 66-116.

Cant NB, Benson CG. Parallel auditory pathways: projection patterns of the different neuronal populations in the dorsal and ventral cochlear nuclei. *Brain Res Bull* 60:457-474, 2003.

Colletti V, Shannon RV. Open set speech perception with auditory brainstem implant? *Laryngoscope* 115:1974-1978, 2005.

Coomes DL, Schofield BR. Separate projections from the inferior colliculus to the cochlear nucleus and thalamus in guinea pigs. *Hear Res* 191:67-78, 2004.

Edgerton BJ, House WF, Hitselberger W. Hearing by cochlear nucleus stimulation in humans. *Ann Otol Rhinol Laryngol Suppl* 91:117-124, 1982.

El-Kashlan HK. Multichannel cochlear nucleus stimulation. *Otolaryngol Head Neck Surg* 121:169-175, 1999.

El-Kashlan HK, Niparko JK, Altschuler RA, Miller JM. Direct electrical stimulation of the cochlear nucleus: surface vs. penetrating stimulation. *Otolaryngol Head Neck Surg* 105:533-543, 1991.

Evans EF, Nelson PG. On the functional relationship between the dorsal and ventral divisions of the cochlear nucleus of the cat. *Exp Brain Res* 17:428-442, 1973.

Faye-Lund H. Inferior colliculus and related descending pathways in rat. *Ups J Med Sci* 93:1-17, 1988.

FitzPatrick KA. Cellular architecture and topographic organization of the inferior colliculus of the squirrel monkey. *J Comp Neurol* 164:185-207, 1975.

Friauf E, Ostwald J. Divergent projections of physiologically characterized rat ventral cochlear nucleus neurons as shown by intra-axonal injection of horseradish peroxidase. *Exp Brain Res* 73:263-284, 1988.

Friesen LM, Shannon RV, Baskent D, Wang X. Speech recognition in noise as a function of the number of spectral channels: comparison of acoustic hearing and cochlear implants. *J Acoust Soc Am* 110:1150-1163, 2001.

Hackney CM, Osen KK, Kolston J. Anatomy of the cochlear nuclear complex of guinea pig. *Anat Embryol (Berl)* 182:123-149, 1990.

Hardie NA, Shepherd RK. Sensorineural hearing loss during development: morphological and physiological response of the cochlea and auditory brainstem. *Hear Res* 128:147-165, 1999.

Harrison JM, Warr WB. A study of the cochlear nuclei and ascending auditory pathways of the medulla. *J Comp Neurol* 119:341-380, 1962.

Heffner RS. Primate hearing from a mammalian perspective. *Anat Rec A Discov Mol Cell Evol Biol* 281:1111-1122, 2004.

Hinkle DE, Wiersma W, Jurs SG. Correlation: A Measure of Relationship. In: *Applied Statistics for the Behavioral Sciences*, 4th Edition, Houghton Mifflin Company, 1998, pp 105-131.

Huang CM, Fex J. Tonotopic organization in the inferior colliculus of the rat demonstrated with the 2-deoxyglucose method. *Exp Brain Res* 61:506-512, 1986.

Jolly CN, Spelman FA, Clopton BM. Quadrupolar stimulation for Cochlear prostheses: modeling and experimental data. *IEEE Trans Biomed Eng* 8:857-865, 1996.

Kelly JB, Masterton, B. Auditory sensitivity of the albino rat. *J Comp Physiol Psychol* 91:930-936, 1977.

Kelly JB, Glenn SL, Beaver CJ. Sound frequency and binaural response properties of single neurons in rat inferior colliculus. *Hear Res* 56:273-280, 1991.

Koppl C, Yates G. Coding of sound pressure level in the barn owl's auditory nerve. *J Neurosci* 19:9674-9686, 1999.

Kuchta J, Otto SR, Shannon RV, Hitselberger WE, Brackmann DE. The multichannel auditory brainstem implant: how many electrodes make sense? *J Neurosurg* 100:16-23, 2004.

Lewicki MS. A review of methods for spike sorting: the detection and classification of neural action potentials. *Network* 9:53-78, 1998.

Lim HH, Anderson DJ. Auditory cortical responses to electrical stimulation of the inferior colliculus: Implications for an auditory midbrain implant. *J Neurophysiol* 96:975-988, 2006.

Lim HH, Anderson DJ. Antidromic activation reveals tonotopically organized projections from primary auditory cortex to the central nucleus of the inferior colliculus in guinea pig. *J Neurophysiol* 97:1413-1427, 2007.

Lorente de Nó. Anatomy of the eighth nerve. The central projection of the nerve endings of the internal ear. *Laryngoscope* 43:1-38, 1933a.

Lorente de Nó. Anatomy of the eighth nerve III. General plan of the structure of the primary cochlear nuclei. *Laryngoscope* 43:327–350, 1933b.

McCreery DB, Agnew WF, Yuen TG, Bullara LA. Charge density and charge per phase as cofactors in neural injury induced by electrical stimulation. *IEEE Trans Biomed Eng* 37:996-1001, 1990.

McCreery DB, Shannon RV, Moore JK, Chatterjee M. Accessing the tonotopic organization of the ventral cochlear nucleus by intranuclear microstimulation. *IEEE Trans Rehabil Eng* 6:391-399, 1998.

McCreery DB, Yuen TG, Bullara LA. Chronic microstimulation in the feline ventral cochlear nucleus: physiologic and histologic effects. *Hear Res* 149:223-238, 2000.

McCreery DB, Lossinsky A, Pikov V. Performance of multisite silicon microprobes implanted chronically in the ventral cochlear nucleus of the cat. *IEEE Trans Biomed Eng* 54:1042-1051, 2007.

Mugnaini E, Warr WB, Osen KK. Distribution and light microscopic features of granule cells in the cochlear nuclei of cat, rat, and mouse. *J Comp Neurol* 191:581-606, 1980a.

Mugnaini E, Osen KK, Dahl AL, Friedrich VL, Jr., Korte G. Fine structure of granule cells and related interneurons (termed Golgi cells) in the cochlear nuclear complex of cat, rat and mouse. *J Neurocytol* 9:537-570, 1980b.

Nayagam DA, Clarey JC, Paolini AG. Powerful, onset inhibition in the ventral nucleus of the lateral lemniscus. *J Neurophysiol* 94:1651-1654, 2005.

Nayagam DA, Clarey JC, Paolini AG. Intracellular responses and morphology of rat ventral complex of the lateral lemniscus neurons in vivo. *J Comp Neurol* 498:295-315, 2006.

Nizami L. Estimating auditory neuronal dynamic range using a fitted function. *Hear Res* 167:13-27, 2002.

Okoyama S, Ohbayashi M, Ito M, Harada S. Neuronal organization of the rat inferior colliculus participating in four major auditory pathways. *Hear Res* 218:72-80, 2006.

Oliver DL. Projections to the inferior colliculus from the anteroventral cochlear nucleus in the cat: possible substrates for binaural interaction. *J Comp Neurol* 264:24-46, 1987.

Osen KK. Cytoarchitecture of the cochlear nuclei in the cat. *J Comp Neurol* 136:453-484, 1969.

Osen KK. Course and termination of the primary afferents in the cochlear nuclei of the cat. An experimental anatomical study. *Arch Ital Biol* 108:21-51, 1970.

Osen KK. Projection of the cochlear nuclei on the inferior colliculus in the cat. *J Comp Neurol* 144:355-372, 1972.

Otto SR, Brackmann DE, Hitselberger WE, Shannon RV, Kuchta J. Multichannel auditory brainstem implant: update on performance in 61 patients. *J Neurosurg* 96:1063-1071, 2002.

Otto SR, Shannon RV, Brackmann DE, Hitselberger WE, Staller S, Menapace C. The multichannel auditory brain stem implant: performance in twenty patients. *Otolaryngol Head Neck Surg* 118:291-303, 1998.

Paolini AG, Clarey JC, Needham K, Clark GM. Fast inhibition alters first spike timing in auditory brainstem neurons. *J Neurophysiol* 92:2615-2621, 2004.

Paolini AG, Clarey JC, Needham K, Clark GM. Balanced inhibition and excitation underlies spike firing regularity in ventral cochlear nucleus chopper neurons. *Eur J Neurosci* 21:1236-1248, 2005.

Paxinos G, Watson C. The Rat Brain in Stereotaxic Coordinates. 5th edition, Academic Press, San Diego, 2005.

Rose JE, Galambos R, Hughes JR. Microelectrode studies of the cochlear nuclei of the cat. *Bull Johns Hopkins Hosp* 104:211-251, 1959.

Roth GL, Aitkin LM, Anderson RA, Merzenich MM. Some features of the spatial organization of the central nucleus of the inferior colliculus of the cat. *J Comp Neurol* 182:661-680, 1978.

Ryugo DK, Willard FH, Fekete DM. Differential afferent projections to the inferior colliculus from the cochlear nucleus in the albino mouse. *Brain Res* 210:342-349, 1981.

Ryugo DK, Pongstaporn T, Wright DD, Sharp AH. Inositol 1,4,5-trisphosphate receptors: immunocytochemical localization in the dorsal cochlear nucleus. *J Comp Neurol* 358:102-118, 1995.

Sachs MB, Abbas PJ. Rate versus level functions for auditory-nerve fibers in cats: tone-burst stimuli. *J Acoust Soc Am* 6:1835:1847, 1974.

Sachs MB, Winslow RL, Sokolowski BH. A computational model for rate-level functions from cat auditory-nerve fibers. *Hear Res* 41:61-69, 1989.

Saint Marie RL, Baker RA. Neurotransmitter-specific uptake and retrograde transport of [3H]glycine from the inferior colliculus by ipsilateral projections of the superior olivary complex and nuclei of the lateral lemniscus. *Brain Res* 524:244-253, 1990.

Schofield BR. Origins of projections from the inferior colliculus to the cochlear nucleus in guinea pigs. *J Comp Neurol* 429:206-220, 2001.

Schofield BR, Cant NB. Projections from the ventral cochlear nucleus to the inferior colliculus and the contralateral cochlear nucleus in guinea pigs. *Hear Res* 102:1-14, 1996.

Schofield BR, Cant NB. Ventral nucleus of the lateral lemniscus in guinea pigs: cytoarchitecture and inputs from the cochlear nucleus. *J Comp Neurol* 379:363-385, 1997.

Schofield BR, Cant NB. Descending auditory pathways: projections from the inferior colliculus contact superior olivary cells that project bilaterally to the cochlear nuclei. *J Comp Neurol* 409:210-223, 1999.

Schwartz MS, Otto SR, Brackmann DE, Hitselberger WE, Shannon RV. Use of a multichannel auditory brainstem implant for neurofibromatosis type 2. Stereotact Funct *Neurosurg* 81:110-114, 2003.

Semple MN, Aitkin LM. Representation of sound frequency and laterality by units in central nucleus of cat inferior colliculus. *J Neurophysiol* 42:1626-1639, 1979.

Shofner WP, Young ED. Excitatory/inhibitory response types in the cochlear nucleus: relationships to discharge patterns and responses to electrical stimulation of the auditory nerve. *J Neurophysiol* 54:917-939, 1985.

Smith PH, Rhode WS. Structural and functional properties distinguish two types of multipolar cells in the ventral cochlear nucleus. *J Comp Neurol* 282:595-616, 1989.

Swadlow HA. Properties of antidromically activated callosal neurons and neurons responsive to callosal input in rabbit binocular cortex. *Exp Neurol* 43:424-444, 1974.

Swadlow HA, Waxman SG, Rosene DL. Latency variability and the identification of antidromically activated neurons in mammalian brain. *Exp Brain Res* 32:439-443, 1978.

Takahashi H, Nakao M, Kaga K. Accessing ampli-tonotopic organization of rat auditory cortex by microstimulation of cochlear nucleus. *IEEE Trans Biomed Eng* 52:1333-1344, 2005.

Thompson AM. Heterogeneous projections of the cat posteroventral cochlear nucleus. *J Comp Neurol* 390:439-453, 1998.

Tolbert LP, Morest DK. The neuronal architecture of the anteroventral cochlear nucleus of the cat in the region of the cochlear nerve root: electron microscopy. *Neuroscience* 7:3053-3067, 1982a.

Tolbert LP, Morest DK. The neuronal architecture of the anteroventral cochlear nucleus of the cat in the region of the cochlear nerve root: Golgi and Nissl methods. *Neuroscience* 7:3013-3030, 1982b.

Warr WB. Fiber degeneration following lesions in the anterior ventral cochlear nucleus of the cat. *Experimental Neurology* 14:453-474, 1966.

Weedman DL, Pongstaporn T, Ryugo DK. Ultrastructural study of the granule cell domain of the cochlear nucleus in rats: mossy fiber endings and their targets. *J Comp Neurol* 369:345-360, 1996.

Yates GK. Basilar membrane nonlinearity and its influence on auditory nerve rate-intensity functions. *Hear Res* 50:145-162, 1990.

Yates GK, Manley GA, Koppl C. Rate-intensity functions in the emu auditory nerve. *J Acoust Soc Am* 107:2143-2154, 2000.

Acknowledgements

We thank Dr. Conor Hogan from the Chemistry department at La Trobe University for assistance in electrochemical activation of the electrodes. We also thank Dr. Karina Needham, Ms. Rebecca Argent and Ms. Courtney Suhr for assistance in histological verification of the electrode sites and comments on the manuscript. This research was conducted at the Auditory Neuroscience Laboratory at the School of Psychological Science, La Trobe University, Australia and the Auditory Clinical Neuroscience Unit, The Bionic Ear Institute, Melbourne, Australia. Funding was provided by the Garnett Passe & Rodney Williams Memorial Foundation and the Bionic Ear Institute.

Figure 1. VCN electrode placements and tonotopic maps. (A) Horizontal representation of the CN along with placement of electrode shanks at their entry point for six out of eight experiments (Key A) verified by histological analysis. (B) (i-vi) Parasagittal representation for the same six experiments in (A) showing the different regions of the CN (AN - Auditory Nerve, VCN – Ventral Cochlear Nucleus, DCN – Dorsal Cochlear Nucleus) along with electrode shank placements (black dashed lines). Black dotted lines indicate approximate location of granule cells close to the free surface of the VCN and the granule cell lamina between the DCN and the VCN in rats (Mugnaini et al., 1980b). Red dotted lines indicate approximate location of layer 2 of the DCN in rats where fusiform cells are found (Mugnaini et al., 1980b). Shown beside these are tonotopic maps obtained in each of the animals. Each of the four shanks is represented by a letter (a-d) and the electrode sites are numbered from 1-8. The colors represent the gradient in frequency with high frequencies shown in red and low frequencies shown in blue (Key B). Each circle on the tonotopic maps and in the parasagittal diagrams represents a recording site on the electrode. Open circles are those sites that did not show any multiunit activity in response to acoustic stimulation. The numbers in the circles correspond to the CF of the multiunit cluster of that site. (C) (i) Photomicrograph of a coronal brain section from Exp 07_005 showing the VCN. Electrode tracks for two of the four shanks are discernable and indicated by arrows. Higher magnification shown in (ii).

Figure 2. Examples of IC electrode placements for three animals. (A-C) Photomicrographs of coronal brain sections with graphical overlays of the different regions of the IC (DCIC – Dorsal Cortex of IC, ECIC – External Cortex of IC, CIC – Central Nucleus of IC), along with electrode placement of two of the identifiable shank tracks (indicated by arrows). Shown beside these are the respective tonotopic maps obtained from each experiment. Each of the four shanks is represented by a letter (a-d) and the electrode sites are numbered from 1-8. The colors represent the gradient in frequency with high frequencies shown in red and low frequencies shown in blue (Key). (D) Schematic representation of electrode placement in the CIC. Vertical dashed lines represent the approximate location of the coronal sections shown in (A), (B) and (C) (1, 2, 3, respectively). Electrodes were inserted along the dorso-ventral axis of the CIC at an approximately 10 degree angle to the vertical.

Figure 3. Acoustic and electrical responses from a CF matched VCN-CIC pair (Exp 002; VCN Site c2; CIC Site a5). (A) PSTHs of CIC site a5 in response to a 10 kHz tone at various SPLs (10 repetitions each SPL, Bin Width = 1 ms). (B) PSTHs of CIC site a5 in response to stimulation of VCN site b2 at various current levels (20 repetitions each current level, Bin Width = 1 ms). Arrow in PSTH at 30 μA indicates time-locked activity corresponding to presumed antidromic activity. (C, D) Response areas of a CF matched pair of multiunit clusters in the VCN and the CIC, respectively. Both sites had a CF of approximately 10 kHz with colors representing normalized spike rate from threshold (blue) to saturation (red). (E) Rate-level functions recorded at CIC site a5 in response to tones at different frequencies (Each frequency is shown by a different color). (F) Electrical thresholds of responses at CIC site a5 to stimulation of multiple VCN sites. Each VCN site is shown by a circle with the color representing the CF of that VCN site. Where two sites in the VCN had the same CF, the thresholds are shown by colored squares. Two VCN sites with CFs of 10 and 21 kHz when stimulated gave no response at CIC site a5 even when stimulated at 100 μA (Not shown). The line joining the lower threshold sites provides an indication of the electrical tuning response. (G) Rate-level functions at CIC site a5 in response to electrical stimulation of VCN sites shown in (F). Colors represent the CFs of the stimulated sites and correspond to the colors indicated in (E) & (F). (H) Electrical response area constructed using data from the lowest threshold VCN sites in (F) & (G); colors show normalized spike rates from threshold (blue) to saturation (red). Solid line corresponds to the range of CF regions stimulated in the VCN.

Figure 4. Horizontal representation of the CN with electrode shanks. Numbers show the percentage of the CF Aligned VCN-CIC pairs on each shank that did not give any response relative to the total CF Aligned pairs on that shank. Shanks on which more than 30% of the pairs gave no response are shown by the open circles while those shanks on which less than 30% gave no responses are shown by the closed circles. Two of the shanks which were not stimulated are indicated by “NS”. One shank that had no CF matches in the CIC is indicated by “NCF”.

Figure 5. Acoustic and electrical response area examples for three different CIC sites. Colors are normalized to spike rate with maximum spike rate represented by red and lowest spike rate represented in light blue. Abrupt ending of the electrical response areas at the low frequency end indicates absence of VCN stimulation sites in that frequency range for a given experiment. Solid lines in the electrical response areas correspond to the range of CF regions stimulated in the VCN.

Figure 6. Classification of rate-level functions and their distributions. (A) Rate-level function types obtained from CIC sites through acoustic stimulation at CF. (B) Rate-level functions obtained from CIC sites to electrical stimulation of CF matched VCN sites. Rate-level responses were classified as either Monotonic (i), Plateau (ii), Non-Monotonic (iii) or Complex (iv). (C) Distribution of response types to acoustic stimulation (left) and electrical stimulation (right). Rate-level functions from only CIC sites which had a CF matched site in the VCN are included in the distribution. Dashed lines in A (i-iv) and B (i-iv) indicate 50% of the maximum firing rate.

Figure 7. Histograms of thresholds (i), saturations (ii) and dynamic ranges in μA (iii) and in decibels (iv) of (A) CF Aligned (n = 289) and (B) Lowest Threshold Aligned (n = 118) VCN-CIC pairs (Bin width = 2 μA; 1 dB). Means, standard deviations (SD), Minimum (Min) and Maximum (Max) values are indicated for each panel.

Figure 8. Correlation between electrical and acoustic thresholds. (A – H) Linear regression lines (dashed) showing comparison of electrical thresholds and acoustic thresholds for 135 CIC sites from all 8 experiments. Data from only CIC sites that responded to stimulation of at least three VCN sites are included. A regression line for all data points in each experiment (thick colored line) is also plotted, with corresponding r value indicated. Asterisks indicate that the r values were significant ($p < 0.05$). (I) Distribution of r values for dashed regression lines shown in (A – H). Colors correspond to the experiment from which the data was derived and are consistent to those used in Figure 1A.

Figure 9. Frequency specificity of CIC activation. (A) Scatter points showing frequency regions stimulated in the VCN versus frequency regions activated in the CIC with lowest threshold. Solid line indicates perfect tonotopic mapping between the VCN & CIC (Ideal case). Closed circles correspond to VCN sites on the Group 1 shanks from which more than 60% of the lowest threshold VCN-CIC pairs gave a mean frequency difference of less than or equal to 3 kHz. VCN sites on the Group 2 shanks from which the lowest threshold VCN-CIC pairs displayed a mean frequency difference of greater than 3 kHz are indicated by the open circles. Crosses indicate scatter points for the two experiments that were not verified histologically. (B) Horizontal representation of the CN showing electrode shank placements at their entry point for Group 1 (closed circles) and Group 2 (open circles) shanks. Numbers for each shank indicate mean frequency difference between all VCN-CIC pairs on the shank that responded with lowest threshold. In two of the shanks, only two VCN-CIC pairs were found indicated by shaded circles (Numbers indicate frequency differences for the two VCN-CIC pairs). In two of other shanks, where the mean frequency difference was greater than 3 kHz, more than 60% of the lowest threshold VCN-CIC pairs gave a frequency difference of less than 3 kHz (Percentages shown next to means) (C) Mean frequency difference for the two groups in (A) & (B). (D) Scatter points showing the CF of each CIC site versus the CF of the VCN site that elicited maximum spike discharge on that CIC site when stimulated across all current levels. Symbols indicate location of the VCN sites (Group 1 shanks, closed circles; Group 2 shanks, open circles; Unknown, crosses). (E) & (F) Histograms of thresholds, saturations and dynamic ranges (μA & dB) for CF Aligned (E) and Lowest Threshold Aligned (F) VCN-CIC pairs for the two groups (Bin width = 2 μA; 1 dB). Mean ± Standard Deviation values are indicated for each panel (Black line/text: Group 1; Gray line/text: Group 2).

Figure 10. Effect of CIC broadness of tuning on frequency specificity. All CIC sites with a Q_{10} factor of less than or equal to one were classified as broadly tuned and those with a Q_{10} factor greater than one were classified as narrowly tuned. Scatter points showing difference in thresholds for all broadly tuned CIC sites (A1) and narrowly tuned CIC sites (B1) from the threshold of a CF matched VCN-CIC pair for each given stimulated VCN site, against their frequency differences from that VCN site. VCN sites belonging to the Group 1 shanks are indicated by the closed circles and those belonging to the Group 2 shanks are indicated by the open circles. Where there was more than one CF matched pair for a given stimulated VCN site, the threshold difference was calculated from the lowest threshold pair. (A2) & (B2) Regression lines (solid lines) with 95% confidence intervals (dashed lines) for the points in (A1) and (B1), respectively, for the Group 1 shanks (black lines) and the Group 2 shanks (gray lines) for broadly and narrowly tuned CIC sites.

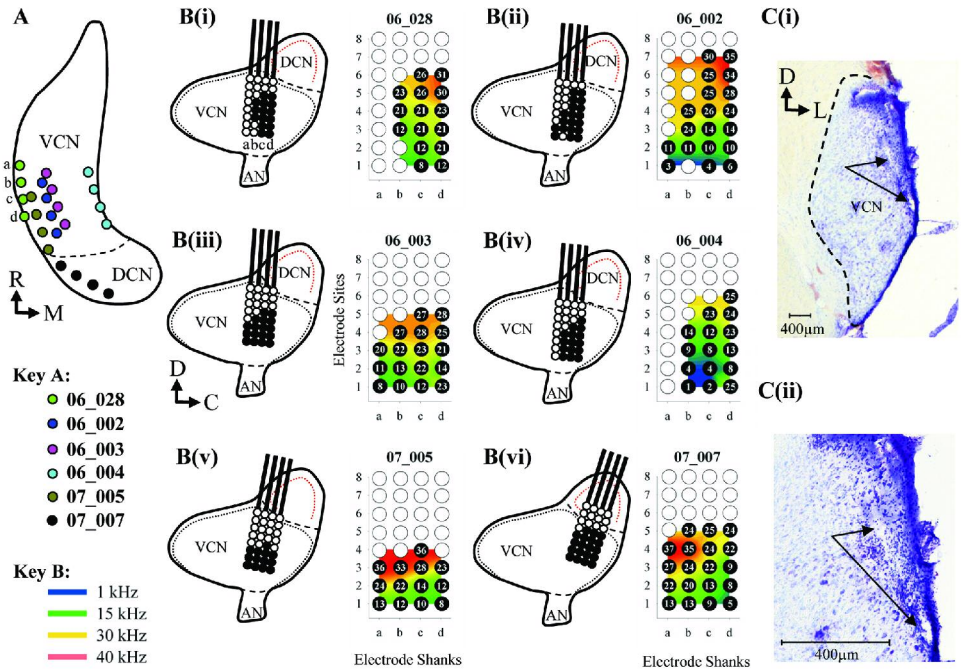

Figure 1. VCN electrode placements and tonotopic maps. (A) Horizontal representation of the CN along with placement of electrode shanks at their entry point for six out of eight experiments (Key A) verified by histological analysis. (B) (i-vi) Parasagittal representation for the same six experiments in (A) showing the different regions of the CN (AN - Auditory Nerve, VCN □ Ventral Cochlear Nucleus, DCN □ Dorsal Cochlear Nucleus) along with electrode shank placements (black dashed lines). Black dotted lines indicate approximate location of granule cells close to the free surface of the VCN and the granule cell lamina between the DCN and the VCN in rats (Mugnaini et al., 1980b). Red dotted lines indicate approximate location of layer 2 of the DCN in rats where fusiform cells are found (Mugnaini et al., 1980b). Shown beside these are tonotopic maps obtained in each of the animals. Each of the four shanks is represented by a letter (a-d) and the electrode sites are numbered from 1-8. The colors represent the gradient in frequency with high frequencies shown in red and low frequencies shown in blue (Key B). Each circle on the tonotopic maps and in the parasagittal diagrams represents a recording site on the electrode. Open circles are those sites that did not show any multiunit activity in response to acoustic stimulation. The numbers in the circles correspond to the CF of the multiunit cluster of that site. (C) (i) Photomicrograph of a coronal brain section from Exp 07_005 showing the VCN. Electrode tracks for two of the four shanks are discernable and indicated by arrows. Higher magnification shown in (ii).

177x125mm (300 x 300 DPI)

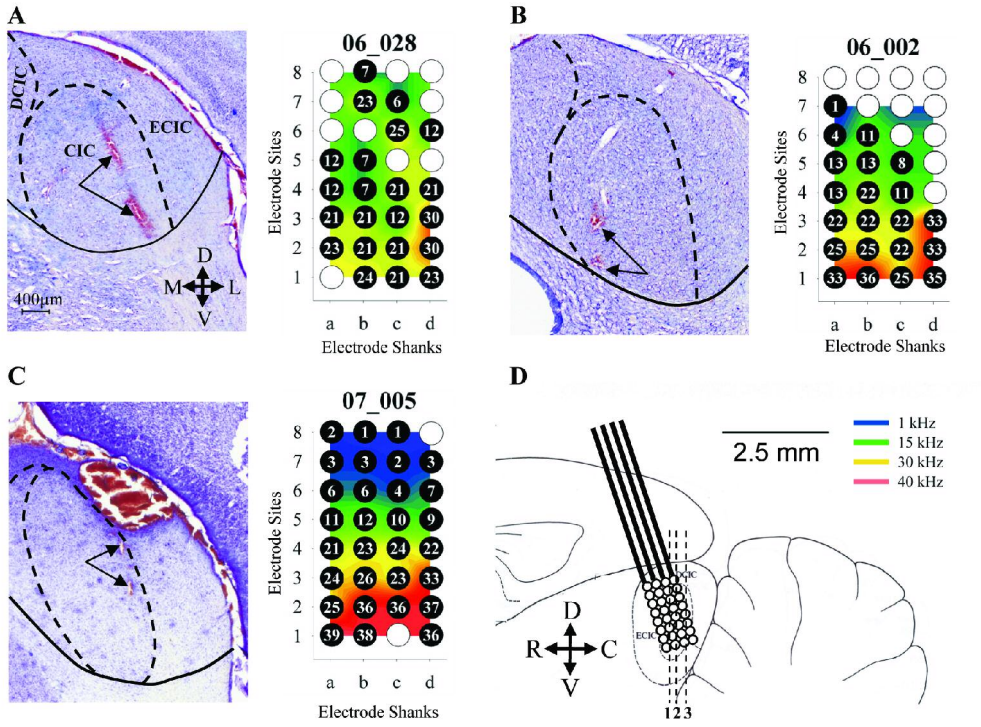

Figure 2. Examples of IC electrode placements for three animals. (A-C) Photomicrographs of coronal brain sections with graphical overlays of the different regions of the IC (DCIC, Dorsal Cortex of IC; ECIC, External Cortex of IC; CIC. Central Nucleus of IC), along with electrode placement of two of the identifiable shank tracks (indicated by arrows). Shown beside these are the respective tonotopic maps obtained from each experiment. Each of the four shanks is represented by a letter (a-d) and the electrode sites are numbered from 1-8. The colors represent the gradient in frequency with high frequencies shown in red and low frequencies shown in blue (Key). (D) Schematic representation of electrode placement in the CIC. Vertical dashed lines represent the approximate location of the coronal sections shown in (A), (B) and (C) (1, 2, 3 respectively). Electrodes were inserted along the dorso-ventral axis of the CIC at an approximately 10 degree angle to the vertical.

163x127mm (300 x 300 DPI)

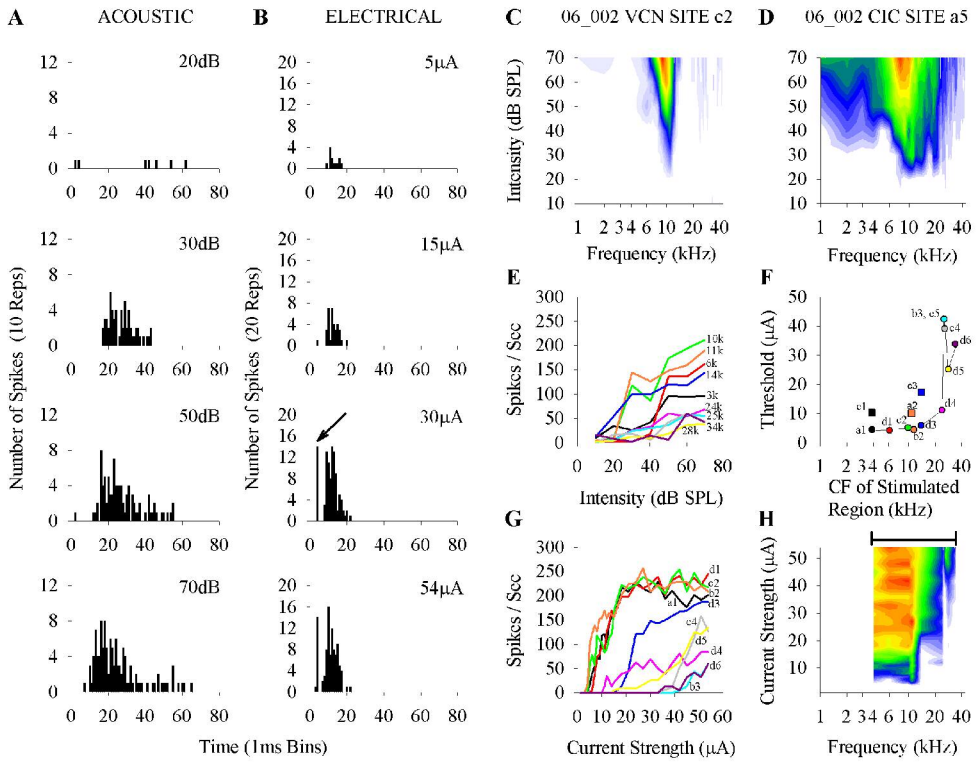

Figure 3. Acoustic and electrical responses from a CF matched VCN-CIC pair (Exp 002; VCN Site c2; CIC Site a5). (A) PSTHs of CIC site a5 in response to a 10 kHz tone at various SPLs (10 repetitions each SPL, Bin Width = 1 ms). (B) PSTHs of CIC site a5 in response to stimulation of VCN site b2 at various current levels (20 repetitions each current level, Bin Width = 1 ms). Arrow in PSTH at 30 μA indicates time-locked activity corresponding to presumed antidromic activity. (C, D) Response areas of a CF matched pair of multiunit clusters in the VCN and the CIC respectively. Both sites had a CF of approximately 10 kHz with colors representing normalized spike rate from threshold (blue) to saturation (red). (E) Rate-level functions recorded at CIC site a5 in response to tones at different frequencies (Each frequency is shown by a different color). (F) Electrical thresholds of responses at CIC site a5 to stimulation of multiple VCN sites. Each VCN site is shown by a circle with the color representing the CF of that VCN site. Where two sites in the VCN had the same CF, the thresholds are shown by colored squares. Two VCN sites with CFs of 10 and 21 kHz when stimulated gave no response at CIC site a5 even when stimulated at 100 μA (Not shown). The line joining the lower threshold sites provides an indication of the electrical tuning response. (G) Rate-level functions at CIC site a5 in response to electrical stimulation of VCN sites shown in (F). Colors represent the CFs of the stimulated sites and correspond to the colors indicated in (E) & (F). (H) Electrical response area constructed using data from the lowest threshold VCN sites in (F) & (G); colors show normalized spike rates from threshold (blue) to saturation (red). Solid line corresponds to the range of CF regions stimulated in the VCN.

368x297mm (150 x 150 DPI)

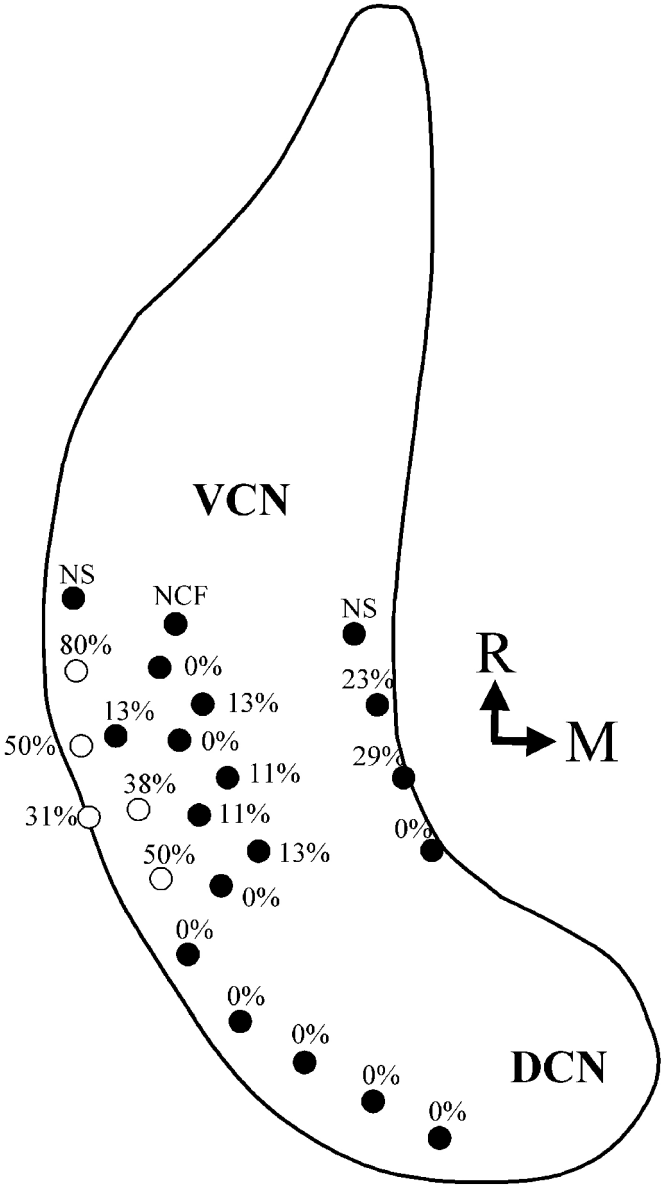

Figure 4. Horizontal representation of the CN with electrode shanks. Numbers show the percentage of the CF Aligned VCN-CIC pairs on each shank that did not give any response relative to the total CF Aligned pairs on that shank. Shanks on which more than 30% of the pairs gave no response are shown by the open circles while those shanks on which less than 30% gave no responses are shown by the closed circles. Two of the shanks which were not stimulated are indicated by □NS□. One shank that had no CF matches in the CIC is indicated by □NCF□.

336x593mm (150 x 150 DPI)

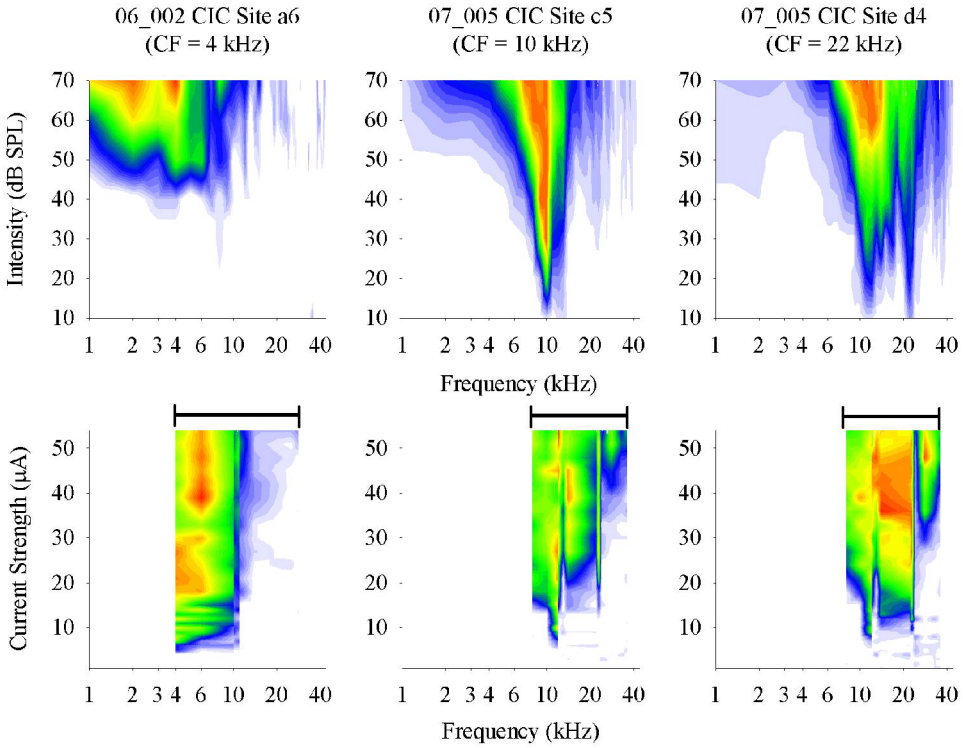

Figure 5. Acoustic and electrical response area examples for three different CIC sites. Colors are normalized to spike rate with maximum spike rate represented by red and lowest spike rate represented in light blue. Abrupt ending of the electrical response areas at the low frequency end indicates absence of VCN stimulation sites in that frequency range for a given experiment. Solid lines in the electrical response areas correspond to the range of CF regions stimulated in the VCN.

303x228mm (150 x 150 DPI)

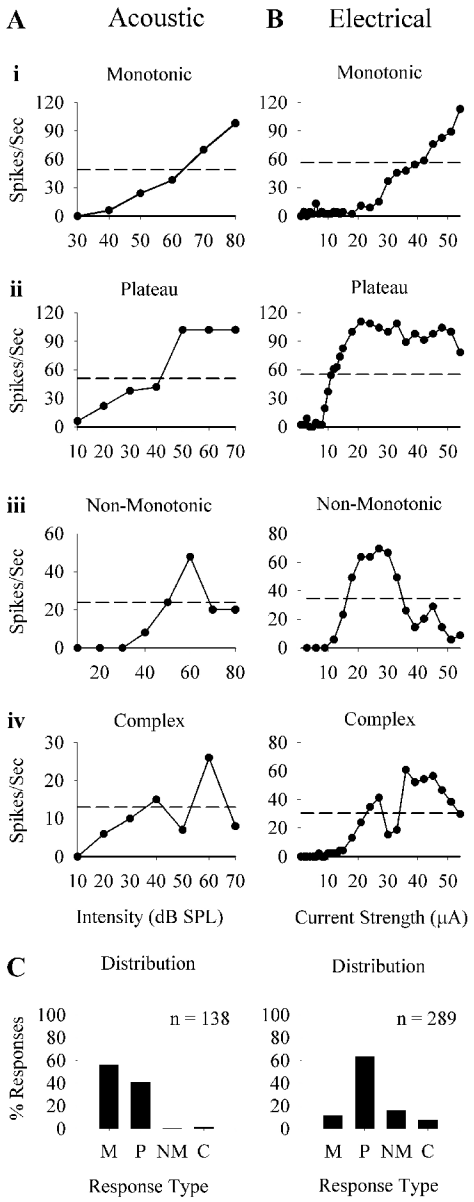

Figure 6. Classification of rate-level functions and their distributions. (A) Rate-level function types obtained from CIC sites through acoustic stimulation at CF. (B) Rate-level functions obtained from CIC sites to electrical stimulation of CF matched VCN sites. Rate-level responses were classified as either Monotonic (i), Plateau (ii), Non-Monotonic (iii) or Complex (iv). (C) Distribution of response types to acoustic stimulation (left) and electrical stimulation (right). Rate-level functions from only CIC sites which had a CF matched site in the VCN are included in the distribution. Dashed lines in A (i-iv) and B (i-iv) indicate 50% of the maximum firing rate.

356x860mm (150 x 150 DPI)

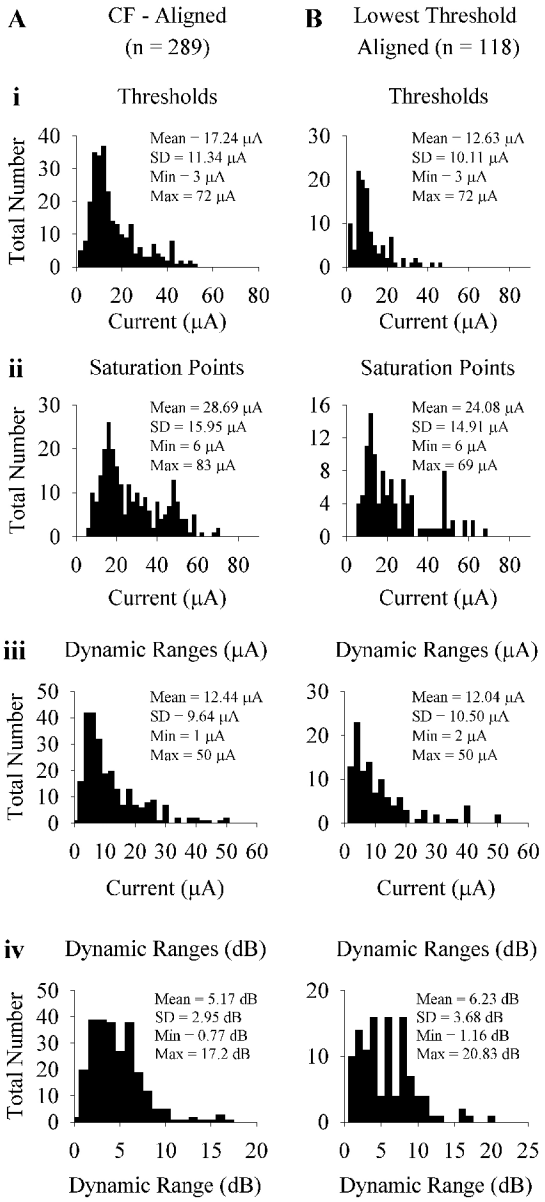

Figure 7. Histograms of thresholds (i), saturations (ii) and dynamic ranges in µA (iii) and in decibels (iv) of (A) CF Aligned (n = 289) and (B) Lowest Threshold Aligned (n = 118) VCN-CIC pairs (Bin width = 2 µA; 1 dB). Means, standard deviations (SD), Minimum (Min) and Maximum (Max) values are indicated for each panel.

358x745mm (150 x 150 DPI)

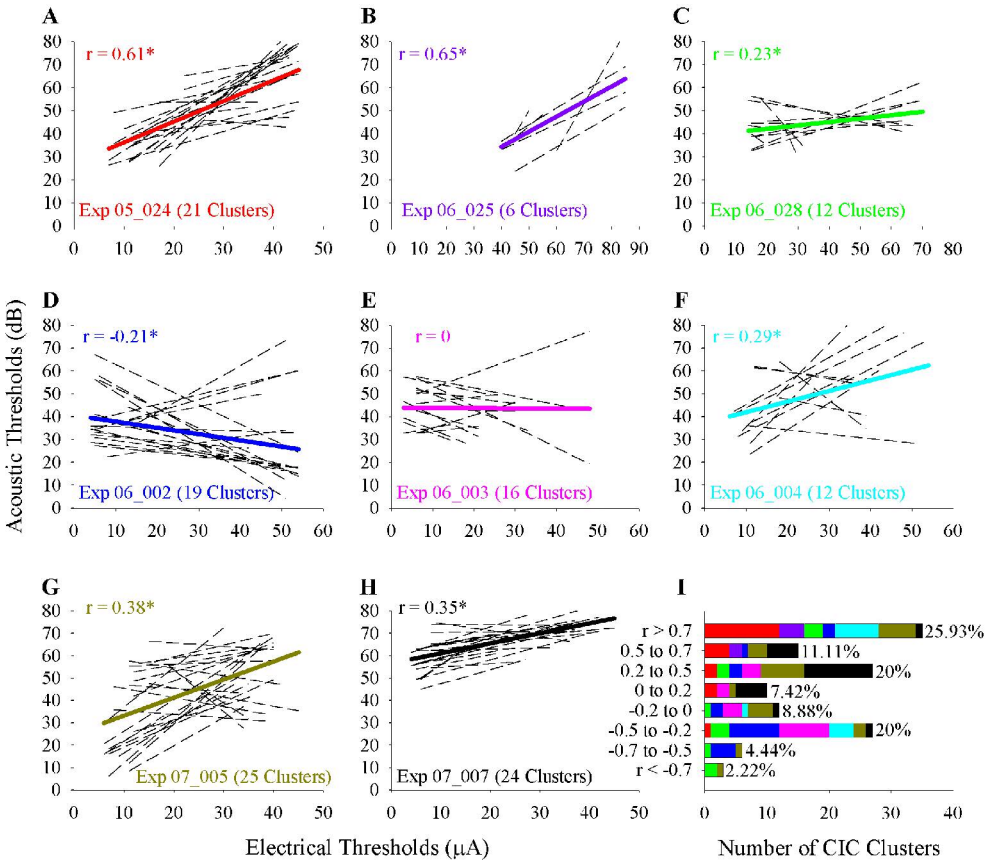

Figure 8. Correlation between electrical and acoustic thresholds. (A □ H) Linear regression lines (dashed) showing comparison of electrical thresholds and acoustic thresholds for 135 CIC sites from all 8 experiments. Data from only CIC sites that responded to stimulation of at least three VCN sites are included. A regression line for all data points in each experiment (thick colored line) is also plotted, with corresponding r value indicated. Asterisks indicate that the r values were significant ($p < 0.05$). (I) Distribution of r values for dashed regression lines shown in (A □ H). Colors correspond to the experiment from which the data was derived and are consistent to those used in Figure 1.

372x321mm (150 x 150 DPI)

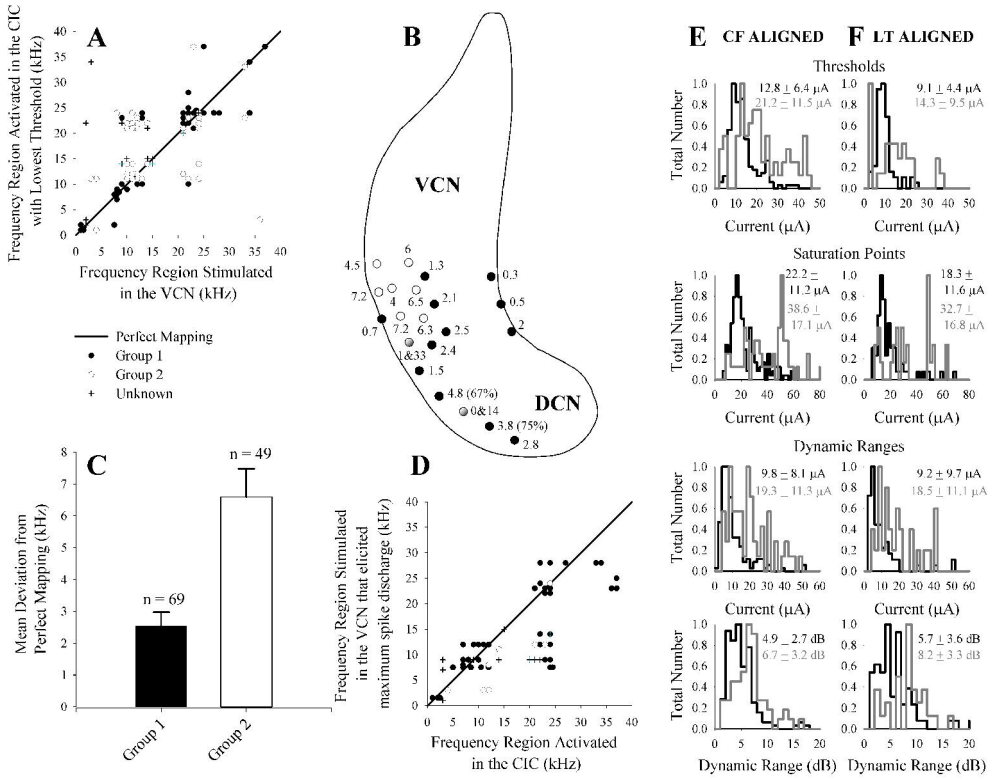

Figure 9. Frequency specificity of CIC activation. (A) Scatter points showing frequency regions stimulated in the VCN versus frequency regions activated in the CIC with lowest threshold. Solid line indicates perfect tonotopic mapping between the VCN & CIC (Ideal case). Closed circles correspond to VCN sites on the Group 1 shanks from which more than 60% of the lowest threshold VCN-CIC pairs gave a mean frequency difference of less than or equal to 3 kHz. VCN sites on the Group 2 shanks from which the lowest threshold VCN-CIC pairs displayed a mean frequency difference of greater than 3 kHz are indicated by the open circles. Crosses indicate scatter points for the two experiments that were not verified histologically. (B) Horizontal representation of the CN showing electrode shank placements at their entry point for Group 1 (closed circles) and Group 2 (open circles) shanks. Numbers for each shank indicate mean frequency difference between all VCN-CIC pairs on the shank that responded with lowest threshold. In two of the shanks, only two VCN-CIC pairs were found indicated by shaded circles (Numbers indicate frequency differences for the two VCN-CIC pairs). In two of other shanks, where the mean frequency difference was greater than 3 kHz, more than 60% of the lowest threshold VCN-CIC pairs gave a frequency difference of less than 3 kHz (Percentages shown next to means) (C) Mean frequency difference for the two groups in (A) & (B). (D) Scatter points showing the CF of each CIC site versus the CF of the VCN site that elicited maximum spike discharge on that CIC site when stimulated across all current levels. Symbols indicate location of the VCN sites (Group 1 shanks, closed circles; Group 2 shanks, open circles; Unknown, crosses). (E) & (F) Histograms of thresholds, saturations and dynamic ranges (µA & dB) for CF Aligned (E) and Lowest Threshold Aligned (F) VCN-CIC pairs for the two groups (Bin width = 2 µA; 1 dB). Mean ± Standard Deviation values are indicated for each panel (Black line/text: Group 1; Gray line/text: Group 2).

783x638mm (150 x 150 DPI)

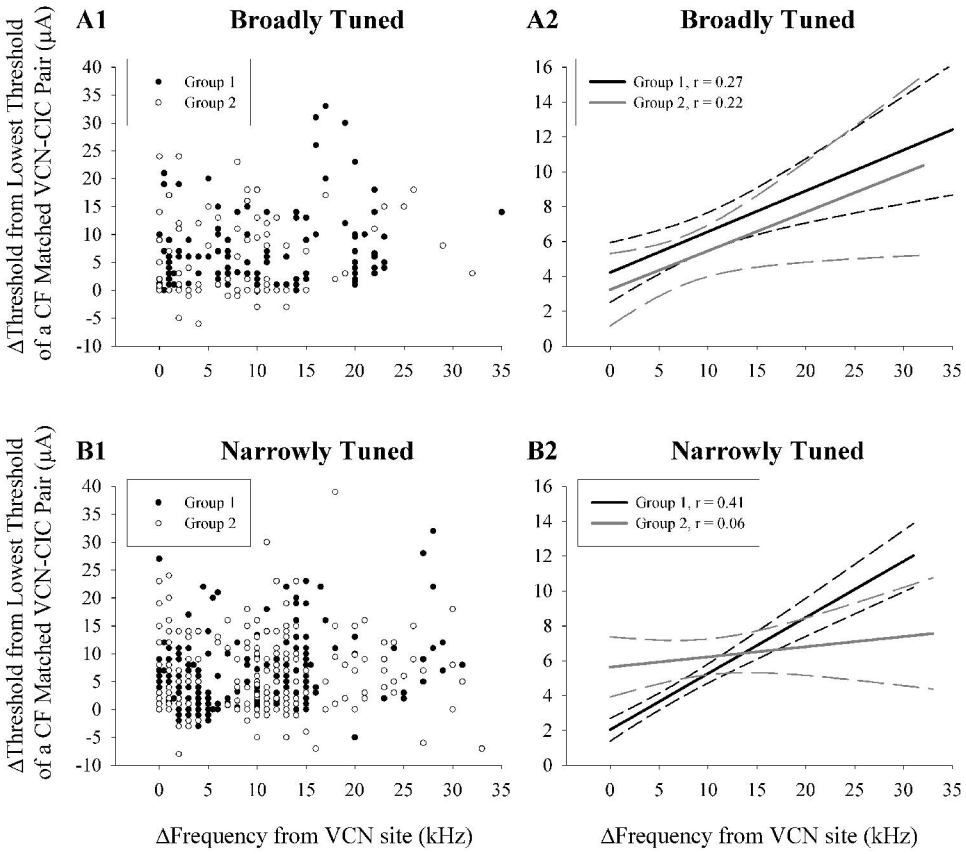

Figure 10. Effect of CIC broadness of tuning on frequency specificity. All CIC sites with a Q_{10} factor of less than or equal to one were classified as broadly tuned and those with a Q_{10} factor greater than one were classified as narrowly tuned. Scatter points showing difference in thresholds for all broadly tuned CIC sites (A1) and narrowly tuned CIC sites (B1) from the threshold of a CF matched VCN-CIC pair for each given stimulated VCN site, against their frequency differences from that VCN site. VCN sites belonging to the Group 1 shanks are indicated by the closed circles and those belonging to the Group 2 shanks are indicated by the open circles. Where there was more than one CF matched pair for a given stimulated VCN site, the threshold difference was calculated from the lowest threshold pair. (A2) & (B2) Regression lines (solid lines) with 95% confidence intervals (dashed lines) for the points in (A1) and (B1) respectively, for the Group 1 shanks (black lines) and the Group 2 shanks (gray lines) for broadly and narrowly tuned CIC sites.
722x620mm (150 x 150 DPI)